


Guided modes and terahertz transitions for two-dimensional Dirac fermions in a smooth double-well potential

R. R. Hartmann ^{*}*Physics Department, De La Salle University, 2401 Taft Avenue, 0922 Manila, Philippines*M. E. Portnoi [†]*Physics and Astronomy, University of Exeter, Stocker Road, Exeter EX4 4QL, United Kingdom
and ITMO University, St. Petersburg 197101, Russia* (Received 27 August 2020; revised 18 October 2020; accepted 9 November 2020; published 30 November 2020)

The double-well problem for the two-dimensional Dirac equation is solved for a family of quasi-one-dimensional potentials in terms of confluent Heun functions. We demonstrate that for a double well separated by a barrier, both the energy-level splitting associated with the wave-function overlap of well states and the gap size of the avoided crossings associated with well and barrier state repulsion can be controlled via the parameters of the potential. The transitions between the two states comprising a doublet, as well as transitions across the pseudogaps are strongly allowed, highly anisotropic, and, for realistic graphene devices, can be tuned to fall within the highly desirable terahertz frequency range.

DOI: [10.1103/PhysRevA.102.052229](https://doi.org/10.1103/PhysRevA.102.052229)

I. INTRODUCTION

The double well in quantum mechanics has been studied in relation to various physical phenomena, ranging from vibrations of polyatomic molecules [1] to applications in Bose–Einstein condensation [2]. Solutions to the Schrödinger equation for smooth double wells are equally broad and have been analyzed using perturbative methods [3], instanton calculus [4], the WKB approximation [5], and other techniques. With the rise of two-dimensional (2D) Dirac materials [6] comes a fresh opportunity to revisit the double-well problem in a relativistic setting and to conduct ultrarelativistic experiments without the need for powerful accelerators. Indeed, there has been significant progress in creating guiding potentials in Dirac materials [7–12], most recently using carbon nanotubes as top gates [13]. These top-gated structures allow the potential profile to be controlled by manipulating the top-gate voltage, allowing the creation of well-defined smooth double wells.

Several approaches have been considered to achieve the goal of confinement in Dirac materials. These range from utilizing magnetic fields [14–18] to implementing Fermi velocity engineering [19–22] to introducing a spatially dependant mass term [23] and, most commonly, using electrostatic potentials [24–47]. Confinement in massless Dirac materials is notoriously difficult due to the Klein tunneling effect [48,49]. However, total confinement can be achieved in such systems for zero-energy states within an electrostatically defined waveguide, whose potential vanishes at infinity. This is because the density of states vanishes outside of the waveguide

[36,39,40,46]. For non-zero-energy states, the bound states within the potential can couple to the continuum states outside the channel and are therefore poorly guided. However, for massive particles, bound states can occur in spite of the Klein phenomena.

The alternative geometry of transmission through potential barriers has also been a subject of extensive research, with the majority of studies utilizing sharp but smooth potentials, i.e., potentials which are steplike or have kinks but are assumed to be smooth on the scale of the lattice constant, so the effects of intervalley scattering are neglected. Supercritical transmission [50–58] and tunneling through barriers has been studied for a variety of one-dimensional (1D) model potentials in both massless and massive 2D Dirac systems [25,27,49,59–76], including square barrier structures such as the double barrier [77–80], inverted double well [81,82], asymmetric waveguides [34,43], and various other steplike structures [41,42,82]. A variety of approaches ranging from the transfer matrix method to the WKB method have been used. However, there is a dearth of studies concerning potentials which span both positive and negative energies, i.e., contain both electronlike and holelike guided modes. The exceptions are periodic potentials [83] and sinusoidal multiple-quantum-well systems [68]. Multiple-quantum-well systems are shown to exhibit transmission gaps in the electrons and holes spectra at tilted angles of incidence [68,84], and the number of oscillations in the transmission window depends on the number of quantum wells. For a double well studied in this paper (see Fig. 1 for the Gedankenexperiment sketch), the width of the transmission gap simply corresponds to the energy difference between guided modes, whereas the oscillations are associated with the splitting of a guided mode into multiple modes due to tunneling between wells. In this paper, we consider the regime where the potential results in an “inversion” of electron and

^{*}richard.hartmann@dlsu.edu.ph[†]M.E.Portnoi@exeter.ac.uk

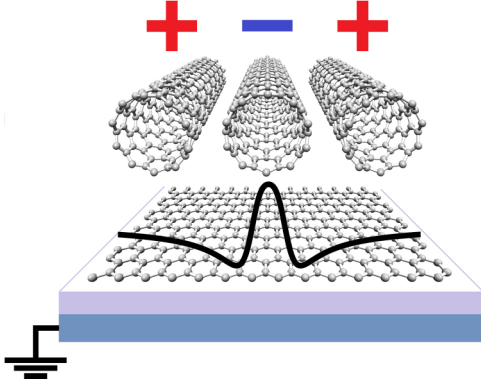


FIG. 1. A schematic diagram of a double-well system, created by three carbon nanotube top gates. The central nanotube is negatively biased to create the central barrier, while the other two are positively biased to create the two wells. The Dirac material sits on top of a dielectric layer (violet layer), which lays on top of the metallic back gate. The Fermi level can be controlled using the back gate potential. The electrostatic potential created by the top gates is shown by the thick black line.

hole states, i.e., the valence band states in the barrier are higher than the conduction band states in the two wells. In this regime, the repulsion of electron and hole states gives rise to interesting features in the eigenvalue spectrum, namely, avoided crossings, which can be controlled via the applied potential. These level avoided crossings also provide a clear physical picture behind the anisotropic energy gap opening near the Dirac point of graphene subjected to a periodic potential [83,85].

The 2D Dirac equation has been the subject of considerable interest due to the explosion of research in transition metal dichalcogenides (TMDs) [86], Weyl semimetals [87], topological insulators [88–90], low-dimensional forms of carbon [91,92], and their silicon analogs [93], for which their low-energy excitations can be described by a Hamiltonian of the form

$$\hat{H} = \hbar v(\hat{k}_x \sigma_x + s_K \hat{k}_y \sigma_y + k_z \sigma_z), \quad (1)$$

where $\hat{k}_x = -i\frac{\partial}{\partial x}$, $\hat{k}_y = -i\frac{\partial}{\partial y}$, $\sigma_{x,y,z}$ are the Pauli spin matrices, v is the Fermi velocity which plays the role of the speed of light, $s_K = \pm 1$ is the valley index number, and k_z is proportional to the particle's in-plane effective mass. For graphene, $v = v_F \approx 10^6$ m/s and $k_z = 0$ [94]. For quasi-1D forms such as narrow-gap carbon nanotubes and certain types of graphene nanoribbons [95,96], the operator \hat{k}_y can be substituted by the number $k_y = E_g/(2\hbar v_F)$, where E_g is the value of the band gap, which can be manipulated via the application of external fields [92,97–101]. Examples of massive 2D Dirac systems include but are not limited to silicene, germanene, TMDs, and graphene on top of lattice-matched boron nitride [102].

The gapless spectrum of graphene and the nearly gapless band structure of narrow-gap carbon nanotubes and ribbons caused a natural attraction to their optical properties in the terahertz (THz) spectral range, which have led to a menagerie of promising applications in the field of THz optoelectronics [92]. The main goal of this paper is to demonstrate that the gate-induced double-well geometry allows for tuneable THz

transitions between the various guided modes. We approach this problem by calculating the dispersion of guided modes in several model potentials which are smooth at the atomic scale, thus allowing us to disregard the problem of valley mixing caused by jumps and kinks in piecewise potentials. These models describe well the shape of an electrostatic potential created in plane by three differently charged nanowires placed above a metallic gate, as can be shown by the mirror charge method.

The detailed calculations of the energy spectrum for a smooth double well, with the middle barrier exceeding the side barriers, are provided in Sec. II, whereas the model potential with a middle barrier below the side barriers is treated in Appendix B. The selection rules for dipole transitions between the guided modes in the potential described in Sec. II are analyzed in Sec. III, followed by the summary of the results in Sec. IV.

II. RELATIVISTIC ONE-DIMENSIONAL DOUBLE-WELL PROBLEM

In what follows, we shall consider a Dirac particle described by the Hamiltonian given by Eq. (1) subject to a double-well 1D potential $U(x)$. Hereafter, the valley index number, s_K , is set to one. The other valley's wave function can be readily obtained by performing a sign change on k_y . The Hamiltonian acts on the two-component Dirac wave function

$$\Psi = \begin{pmatrix} \psi_A(x) \\ \psi_B(x) \end{pmatrix} e^{ik_y y} \quad (2)$$

to yield the coupled first-order differential equations

$$(V - E + \Delta_z)\psi_A - i\left(\frac{d}{d\tilde{x}} + \Delta_y\right)\psi_B = 0 \quad (3)$$

and

$$(V - E - \Delta_z)\psi_B - i\left(\frac{d}{d\tilde{x}} - \Delta_y\right)\psi_A = 0, \quad (4)$$

where $\tilde{x} = x/L$ and L is a constant with the dimension of length. $V = UL/\hbar v_F$ and the charge carrier energy, ε , have been scaled such that $E = \varepsilon L/\hbar v_F$. The charge carriers propagate along the y direction with wave vector $k_y = \Delta_y/L$, which is measured relative to the Dirac point and $\Delta_z = k_z L$ represents their effective mass in dimensionless units. Finally, $\psi_A(x)$ and $\psi_B(x)$ are the wave functions associated with the A and B sublattices, respectively. Substituting $\psi_A = \frac{1}{2}(\psi_1 e^{\frac{1}{2}i\phi} + \psi_2 e^{-\frac{1}{2}i\phi})$ and $\psi_B = \frac{1}{2}(\psi_1 e^{\frac{1}{2}i\phi} - \psi_2 e^{-\frac{1}{2}i\phi})$, where $\phi = \arctan(\Delta_y/\Delta_z)$, allows Eqs. (3) and (4) to be reduced to a single second-order differential equation in ψ_j :

$$-\frac{d^2\psi_j}{dZ^2} + V_{s_j}\psi_j = M^2\psi_j, \quad (5)$$

where

$$V_{s_j}(Z) = W^2(Z) - s_c s_j \frac{dW(Z)}{dZ} \quad (6)$$

and the other spinor component is found by the relation

$$\psi_{j'} = -\frac{1}{M} \left(V - E + s_c s_j \frac{d}{dZ} \right) \psi_j, \quad (7)$$

where $\tilde{x} = s_c iZ$, $s_c = \pm 1$, $W = V - E$, $s_j = (-1)^j$, and $j = 1, 2$ ($j' = 2, 1$) corresponds to the spinor components ψ_1 (ψ_2) and ψ_2 (ψ_1), respectively. In this basis, the particle's transverse momentum Δ_y and in-plane effective mass Δ_z have been combined into a single effective mass, $M = \sqrt{\Delta_y^2 + \Delta_z^2}$. Equation (5) is of the same form as the Schrodinger equation, i.e., a second-order differential equation with no first-order derivative. Therefore, if V_{s_j} is equal to a potential possessing known solutions to the Schrödinger equation, then for zero-energy states, we can readily write down the bound state spectrum of the potential, W , which satisfies the nonlinear Eq. (6) [103–105]. It should also be noted that for zero-energy modes, the left-hand side of Eq. (5) is of the form of the super-Hamiltonian, W plays the role of the superpotential, and the allowed M plays the role of the energy eigenstates [103,104]. Thus there exists a plethora of potentials which admit solutions for zero-energy modes. These zero-energy modes are highly relevant to the study of electronic waveguides formed by graphene top-gated structures [13,36]. In pristine graphene, waveguides formed by potentials which vanish at infinity possess fully guided modes only at zero energy, at nonzero energy the guided modes are leaky. Since there is a threshold value in the characteristic strength of the confinement potential (controlled by the applied gate voltage), for which the first zero-energy bound mode appears, such structures can be utilized as the basis of switchable devices, thus overcoming the problem of minimal conductivity, which is a major obstacle in graphene applications for digital electronics. For nonzero energy, the W which satisfies the nonlinear Eq. (6) for a given potential V_{s_j} will be eigenvalues of an energy-dependent potential [106]. However, we are interested in potentials which are independent of energy and are suitable for the use of modeling double wells in Dirac materials.

In what follows, we consider the case where the 2D Dirac equation reduces to the confluent Heun equation for a family of potentials, some of which can be used to describe a double well separated by a barrier. This quantum model is quasiexactly solvable [39,46,107–112], i.e., only a subset of the eigenvalues can be found explicitly. We study bound states contained within double-well potentials and calculate their entire energy spectrum. Energy-level splitting associated with quantum tunneling between wells and avoided crossings associated with the intermixing of electron-hole states are discussed. Finally, THz applications utilizing the doublet states and avoided crossing points are considered.

We seek to recast Eq. (5) in the form of the normal symmetrical confluent Heun equation [113]. This can be achieved by applying the transformation $\xi = \xi(Z)$ to the independent variable and $\psi_j = \exp[-\int \frac{1}{2}(\frac{d\Phi}{d\xi})d\xi] \Psi_{s_j, s_c}(\xi)$, where $\Phi = \frac{d\xi(Z)}{dZ}$, to the dependent variable. If the potential is of the form

$$V = \frac{a_2 \xi^2 + a_1 \xi + a_0}{1 - \xi^2} \Phi_{\eta_1, \eta_2}, \quad (8)$$

where a_2 , a_1 , and a_0 are constants, $\Phi_{\eta_1, \eta_2} = C_{\eta_1, \eta_2} (1 - \xi)^{\eta_1} (1 + \xi)^{\eta_2}$, η_1 and η_2 can take the values of unity or zero, and C_{η_1, η_2} is a constant, then Eq. (5) reduces to the normal symmetrical form of the Confluent Heun

equation (see Appendix A):

$$-\frac{d^2 \Psi_{s_j, s_c}}{d\xi^2} + \left[p^2 + \frac{\lambda - 2p\beta\xi}{\xi^2 - 1} + \frac{m^2 + s^2 - 1 + 2ms\xi}{(\xi^2 - 1)^2} \right] \Psi_{s_j, s_c} = 0. \quad (9)$$

If the parameters η_1 and η_2 defining Φ_{η_1, η_2} are not set to zero or unity, then the aforementioned transformations will result in an equation different from Eq. (9), which is the basis of the method used in this paper. Equation (8) provides a family of energy-independent potentials for which the quasi-1D Dirac problem admits wave functions in terms of the confluent Heun functions. Notable members of this family include the Rosen-Morse potential, a generalized Hulthen-like potential, and the shifted 1D Coulomb potential (see Appendix A for further details).

One of the opportunities to describe a smooth double well is to choose the case of $\eta_1 = \eta_2 = 0$. We require that our potential is nonsingular and vanishes as $x \rightarrow \pm\infty$. Therefore we set $a_2 = 0$ and the potential becomes

$$V = \frac{a_1 Z + a_0}{1 - Z^2} \equiv \frac{A_1 \tilde{x} + A_0}{1 + \tilde{x}^2}, \quad (10)$$

where the potential parameters A_1 and A_0 are related to the parameters appearing in Eq. (9) via the relations

$$p = s_p \sqrt{E^2 - M^2}, \quad \beta = -is_c A_1 E / p,$$

$$\lambda = -A_1(A_1 + is_j) + 2EA_0,$$

$$\Lambda_{1,2} = s_a A_0, \quad \Lambda_{2,1} = is_a(A_1 + is_j)s_c,$$

where $\Lambda_1 = m$, $\Lambda_2 = s$, and $s_{a,p} = \pm 1$. Equation (10) is a linear combination of the Lorentzian and its logarithmic derivative, which has known solutions for the radial Dirac equation [37]. Since the potential given by Eq. (10) is smooth and vanishes as $x \rightarrow \pm\infty$, it may be utilized for modeling top-gated structures in 2D Dirac materials. The Lorentzian has already been used to model the potential generated by a top gate formed by a carbon nanotube [13]. It should also be noted that when $p = 0$, i.e., $|E| = M$, the Lorentzian admits exact energy eigenvalues (see Appendix C). Exponentially decaying potentials also play an important role in the modeling of heterostructure devices based upon zero-energy modes in Dirac materials, as these potentials are often quasiexact, admitting some exact energy eigenvalues. As mentioned previously in the Introduction, the majority of work on multiple-barrier structures focus on smooth but sharp potentials. However, realistic potential profiles vary slowly over the length scale of the Dirac material's lattice constant and discontinuous potentials have yet to be realized. Furthermore, many piecewise potentials do not result in smooth wave functions across the whole of configuration space due to the nontrivial nature of their boundary conditions [42,43,114]. Smooth potentials do not suffer from this problem [36,39,46,115], additionally they permit intervalley scattering to be neglected.

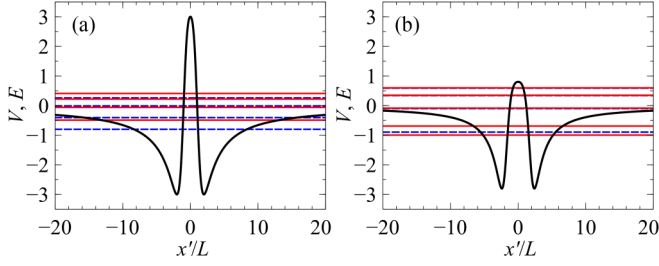


FIG. 2. Energy levels of 2D Dirac electrons in a double-well potential. The black solid lines show the two potentials given by Eq. (10), (a) for the case of $A_1 = -6$ and $A_0 = 0$ and (b) for the case of $A_1 = -3$ and $A_0 = -2$. The horizontal lines depict the bound-state energies for the four lowest doublet states, plus all the holelike states in the spectrum for the case of $M = 1$. The red solid and blue dashed lines correspond to the eigenvalues of the even and odd modes of ψ_I , respectively.

The stationary points, \tilde{x}_s , of the potential Eq. (10) are located at

$$\tilde{x}_s = -r + s_r \sqrt{1 + r^2}, \quad (11)$$

where $r = A_0/A_1$ and $s_r = \pm 1$. Making the coordinate transformation $\tilde{x} = |x'| + \tilde{x}_s$ allows the potential Eq. (10) to be utilized as a model for quasi-1D double wells in realistic top-gated Dirac material heterostructures. When $A_1 < 0$ and $s_r = -1$, the potential is a double well (see Fig. 2) whose local minima are located a distance of $2\sqrt{1 + r^2}$ apart. The two wells of depth $A_1/(2\tilde{x}_1)$ are separated by a barrier of height $A_1/(2\tilde{x}_{-1})$, which acts as a single well for holelike particles, with the possible experimental setup shown in Fig. 1. Although we are dealing with a single-particle Hamiltonian, it is convenient to call the states with the energy growing with increasing $|\Delta_y|$ when $|\Delta_y| \rightarrow \infty$ as electronlike states or electrons, whereas the holelike states correspond to $E \rightarrow -\infty$ when $|\Delta_y| \rightarrow \infty$. In the limit that $r \gg 1$, the central barrier's height becomes negligible in comparison to the depth of the two wells. Conversely, when $A_1 > 0$ and $s_r = -1$, the potential becomes a single electron well, lying between two barriers, which act as a double well for holelike particles. It should be recalled that the potential described by Eq. (10) is scaled such that $V = UL/\hbar$, where L is the effective width of the potential. Therefore, the dimensionless parameters A_1 and A_0 , which enter Eq. (10), are related to the effective potential width and depth. It can be shown both via relativistic Levinson's theorem [58,116–118] and analytically [36,46] that the number of bound states contained within a realistic confining potential is defined by the product of the potential's depth and its width, rather than its exact form. Therefore, the parameters A_0 and A_1 can be extracted from existing single waveguide systems by experimentally observing the appearance of the first bound state as the potential depth is increased beyond the critical threshold [13]. Although the effective width of the potential is governed by technological limitations, mostly by the separation of the top gate from the Dirac material, the parameters A_1 and A_0 can still be controlled by the voltages applied to the top gates.

Let us now calculate the energy spectrum of bound states contained within a double well separated by a barrier, de-

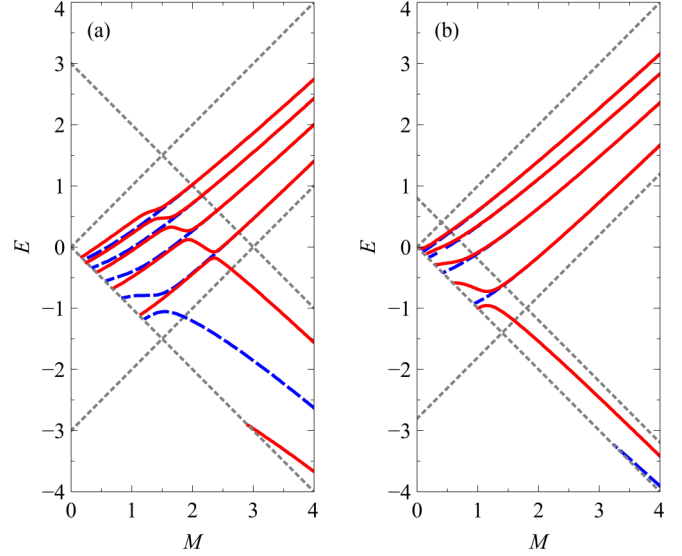


FIG. 3. The energy spectrum of bound states contained within a double well separated by a barrier, defined by the potential parameters (a) $A_1 = -6$ and $A_0 = 0$ and (b) $A_1 = -3$ and $A_0 = -2$, as a function of effective mass, M . Here, only the four lowest doublet states are displayed and all barrier states are present within the energy range shown. The alternating red solid and blue dashed lines represent the even (odd) and odd (even) modes of ψ_I (ψ_{II}), respectively. The boundary at which the bound states merge with the continuum is denoted by the grey short dashed lines.

scribed by Eq. (10). The solution to Eq. (5) for ψ_1 and its corresponding ψ_2 can be written as (see Appendix A)

$$\psi_1 = \sum_{s_c, c_p, s_a} C_{s_c, c_p, s_a} \left(-\frac{s_a + A_0 + i s_c A_1}{2M} \right)^{-\frac{s_c s_a}{2}} \Psi_{-1, s_c} \quad (12)$$

and

$$\psi_2 = \sum_{s_c, c_p, s_a} C_{s_c, c_p, s_a} \left(-\frac{s_a + A_0 + i s_c A_1}{2M} \right)^{\frac{s_c s_a}{2}} \Psi_{1, s_c}, \quad (13)$$

respectively, where $\Psi_{s_j, s_c} = (1 - \xi)^{\frac{\gamma}{2}} (1 + \xi)^{\frac{\delta}{2}} e^{-p\xi} u(\frac{1-\xi}{2})$, and $u = u(p, \alpha, \gamma, \delta, \sigma; \frac{1-\xi}{2})$ are the Heun Confluent functions [113] whose parameters are defined as $\gamma = m + s + 1$, $\delta = m - s + 1$, $\alpha = -\beta + m + 1$, $\sigma = \lambda - 2p(\beta - \gamma) - m(m + 1)$, $m = s_a A_0$, $s = i s_a (A_1 + i s_j) s_c$, and C_{s_c, c_p, s_a} are weighting coefficients. For bound states, we require that the term $e^{-p\xi}$ decays as $x \rightarrow \infty$; this imposes two conditions: First $s_p = s_c$, and second, the absolute value of the particle's energy must be less than the reduced mass, i.e., $|E| < |M|$. The functions ψ_1 and ψ_2 are neither even nor odd. For understanding optical selection rules and for a more clear mapping of our results to the conventional double well picture, we shall move to the symmetrized basis functions $|\psi_I\rangle = |\psi_1\rangle - |\psi_2\rangle$ and $|\psi_{II}\rangle = -i(|\psi_1\rangle + |\psi_2\rangle)$. It should be noted that in this basis, an exchange of the signs of V and E is formally equivalent to exchanging ψ_I with ψ_{II} for the original V and E . Therefore, inverting the potential only results in a sign change of the eigenvalues. In the symmetrized basis, one can construct a linear combination of functions Eqs. (12) and (13)

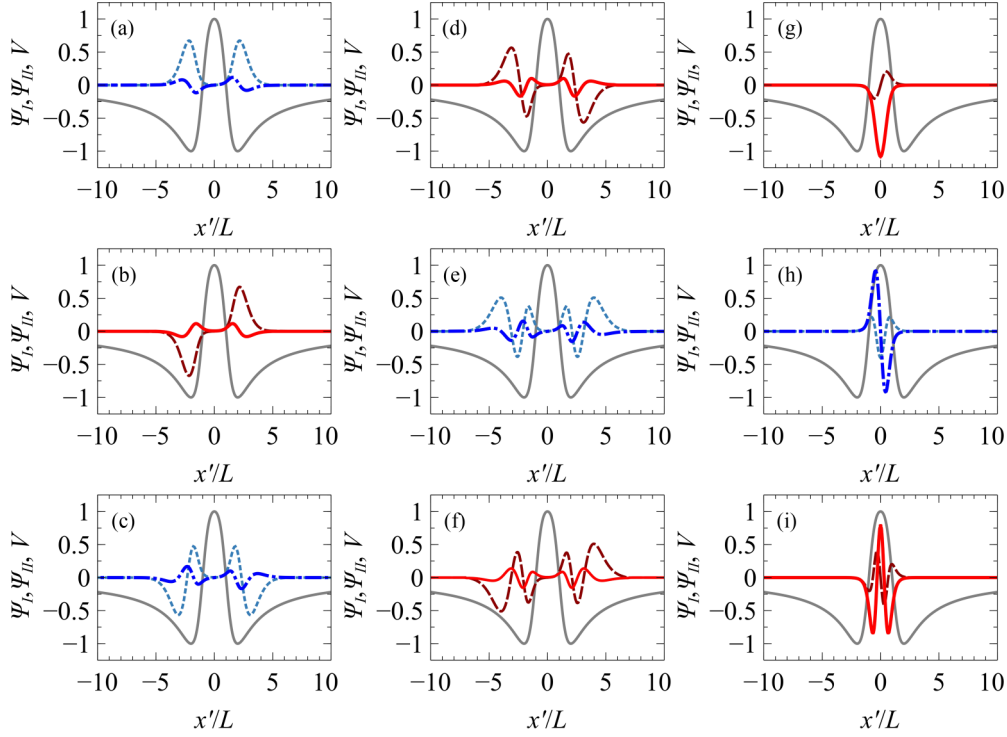


FIG. 4. The normalized bound-state wave functions of the double-well potential. $V = A_1 \tilde{x}/(1 + \tilde{x}^2)$, where $\tilde{x} = |x'| - 1$, $A_1 = -6$, and $M = 3.5$ for the first three doublet states of energies: (a) $E = 0.92814$, (b) $E = 0.92818$, (c) $E = 1.54719$, (d) $E = 1.54723$, (e) $E = 1.98230$, (f) $E = 1.98235$, and for the hole states of energy (g) $E = -1.10843$, (h) $E = -2.23465$, and (i) $E = -3.31137$. The solid red and dash-dotted blue lines correspond to the even and odd modes of Ψ_I , respectively, while the dashed and short dashed lines correspond to the other spinor component Ψ_{II} . The grey line shows the double-well potential as a guide to the eye, plotted in arbitrary units.

to form solutions which are electron- ($s_a = 1$) and holelike ($s_a = -1$),

$$\psi_I = \sum_{s_a} D_{s_a} \text{Im}(\rho^* \Psi_{1,1} + \rho^{-1} \Psi_{1,-1}), \quad (14)$$

$$\psi_{II} = \sum_{s_a} D_{s_a} \text{Re}(\rho^* \Psi_{1,1} + \rho^{-1} \Psi_{1,-1}), \quad (15)$$

where Re and Im are the standard notations for the real and imaginary parts of a complex number, $\rho = (-2M)^{-\frac{s_a}{2}} (s_a + A_0 - iA_1)^{\frac{s_a}{2}}$ and D_{s_a} are the weighting constants. For bound states, we require that the spinor components, Eqs. (14) and (15), vanish at infinity, i.e., $\psi_{I,II}(x' \rightarrow \pm\infty) = 0$, while the coordinate transformation, $\tilde{x} = |x'| + \tilde{x}_s$, imposes the continuity condition

$$\psi_I(\tilde{x}_-) = 0 \quad (16)$$

for odd states and

$$\left. \frac{\partial \psi_I}{\partial x} \right|_{\tilde{x}_-} = 0 \quad (17)$$

for even states. The coordinate transformation also requires that $\psi_{I,II}(x') = -\psi_{I,II}(-x')$ and $\psi_{I,II}(x') = \psi_{I,II}(-x')$ for odd and even states, respectively. However, the radius of convergence, of the power series, is unity. Therefore, an iterative, analytic continuation method must be employed to evaluate the confluent Heun function beyond its radius of convergence [119]. First, the power series u is evaluated at the point $\tilde{\xi}_1$, which lies within the radius of convergence. A new series

expansion is then performed about the point $\tilde{\xi}_1$, which in turn is used to evaluate the point $\tilde{\xi}_2$, and so on and so forth. This allows the energy eigenvalues to be found via a simple shooting method [120,121] which utilizes the wave functions of Eqs. (12) and (13).

In Fig. 3, we plot the energy spectrum of bound states (square integrable along the x direction) defined by the potential parameters $A_1 = -6$ and $A_0 = 0$, as a function of effective mass, M , displaying only the four lowest lying electronlike doublets and all the holelike states within the energy range. When $E \ll M + V_{\min}$ (where V_{\min} is the minimum value of the potential), the spectrum resembles a single, holelike particle trapped within a positive potential barrier. The highest in energy holelike branch is s -like (nodeless) for ψ_I , and the number of nodes increases by one as the branches progress toward more negative energies. For $E \gg -M + V_{\max}$ (where V_{\max} is the maximum value of the potential), the spectrum is electronlike and the energy splittings of the doublets (each shown by a red line with a blue line underneath in Fig. 3) tend to zero with increasing M , as expected for nonrelativistic particles when increasing mass suppresses tunneling. In this regime, it can be seen from Fig. 4 that the particles are localized in the region of the wells, and that the wave functions behave as a linear combination of the wave functions associated with the individual wells. This gives rise to two states where there would have been one if tunneling was forbidden. For ψ_I , the number of nodes increases by one as the branches progress to higher energies. However, since ψ_{II}

is related to the derivative of ψ_I and the potential is even in x , i.e., $V(-x) = V(x)$, the asymmetric linear combination of the two single well functions forces a node in the barrier between them, while the symmetric combination does not, which is reflected in the behavior of ψ_{II} being precisely the same as a wave function for a nonrelativistic particle in a double well, whereas, the component ψ_I has the opposite parity. Finally, in the energy zone $M - V_{\min} < E < -M + V_{\max}$, the solutions are a linear combination of electronlike and holelike states. It can be seen from see Fig. 3 that a series of avoided crossings are opened in the energy spectrum due to the repulsion of barrier and well-doublet states. Also, in this energy zone, the energy-level splitting associated with quantum tunneling increases until the bound states merge with the continuum states. This energy splitting between the two doublets can be controlled in realistic Dirac-material-heterostructures by either adjusting the strength of the applied top-gate voltages or by the choice of geometry. This, coupled with the ability to change the position of the Fermi level via a back gate, gives rise to many possible device applications. Indeed, utilizing the dependence on the number of zero-energy modes on potential strength in single-well smooth electron waveguides has been proposed as the basis switching devices in graphene [36].

III. TERAHERTZ TRANSITIONS

Within this section, we provide the general formalism for calculating the dipole matrix element of THz transitions between guided modes of quasiparticles described by the Hamiltonian given by Eq. (1). For a Dirac particle subject to a 1D potential $U(x)$, the unperturbed Hamiltonian is given by $\hat{H}_0 = \hat{H} + \mathbf{I}U_z$ and the corresponding eigenfunctions of the unperturbed Hamiltonian are given by $(\psi_A(x), \psi_B(x))^T e^{ik_x y} / \sqrt{N}$, where N is a normalization factor given by the expression $N = l \int_{-\infty}^{\infty} (|\psi_A|^2 + |\psi_B|^2) dx$, and l is the sample length. In the presence of an electromagnetic field, the particle momentum operator, $\hat{\mathbf{p}}$, is modified such that $\hat{\mathbf{p}} \rightarrow \hat{\mathbf{p}} + e\mathbf{A}/c$, where e is the elementary charge, and \mathbf{A} is the magnetic vector potential, which is related to $\hat{\mathbf{e}} = (e_x, e_y)$, the unit vector describing the polarization of the electromagnetic wave, via the relation $\mathbf{A} = A\hat{\mathbf{e}}$. For linearly polarized light, the polarization vector is expressed as $(\cos(\varphi_0), \sin(\varphi_0))$, while for right- and left-handed polarized light it is $(1, -i)/\sqrt{2}$ and $(1, i)/\sqrt{2}$, respectively. The general form of the perturbation due to an electromagnetic wave impinging normally to a Dirac material is

$$\delta H = \frac{eAv_F}{c} (\sigma_x e_x + s_K \sigma_y e_y). \quad (18)$$

Using the wave functions given in Eq. (2), in the limit that $l \rightarrow \infty$ the matrix element of transition becomes

$$|\langle f | \delta H | i \rangle| = G_1 \left| \int_{-\infty}^{\infty} [(e_x - is_K e_y) \psi_{A,f}^* \psi_{B,i} + (e_x + is_K e_y) \psi_{B,f}^* \psi_{A,i}] dx \right| \delta_{k_{y,i}, k_{y,f}}, \quad (19)$$

where $G_1 = eAv_F / (c\sqrt{N_i N_f})$ and the indices i and f correspond to the initial and final states, respectively. For free 2D massless Dirac fermions, Eq. (19) becomes valley independent [122] while, in contrast, massive 2D Dirac fermions

have valley-dependent optical transition rules [101]. We shall now analyze the optical selection rules between guided modes contained within the electrostatically controlled double well defined by Eq. (10). To do so, it is more convenient to move from the original $|\psi_A\rangle, |\psi_B\rangle$ basis to the symmetrized one. The functions ψ_A and ψ_B can be expressed in terms ψ_I and ψ_{II} via the transformation $(\psi_A, \psi_B)^T = U(\psi_I, \psi_{II})^T$, where

$$U = \frac{1}{2} \begin{pmatrix} i \sin(\frac{1}{2}\phi) & i \cos(\frac{1}{2}\phi) \\ \cos(\frac{1}{2}\phi) & -\sin(\frac{1}{2}\phi) \end{pmatrix}. \quad (20)$$

To shift to the symmetrized basis, we make a unitary transformation to δH with the unitary operator U . Under this change, the perturbation δH transforms as $\delta \check{H} = U^\dagger \delta H U$:

$$\delta \check{H} = -\frac{ev_F A}{4c} \left(e_x \sigma_y + \frac{s_K e_y \Delta_z}{\sqrt{\Delta_z^2 + \Delta_y^2}} \sigma_x + \frac{e_y \Delta_y}{\sqrt{\Delta_z^2 + \Delta_y^2}} \sigma_z \right). \quad (21)$$

The optical transitions between different guided modes can be categorized into two distinct groups. First, when the parity of each of the symmetrized spinor components ψ_I and ψ_{II} is preserved during the transition, i.e., both $\psi_{I,i}$ and $\psi_{I,f}$ are even, or both odd. Second, when the parity of each component changes after the transition, i.e., $\psi_{I,i}$ is odd (even) while $\psi_{I,f}$ is even (odd). When a transition, which preserves the parity of each spinor component, occurs, its matrix element, given by Eq. (19), can be expressed in terms of the symmetrized spinor components, Eqs. (14) and (15) as

$$|\langle f | \delta H | i \rangle| = G_2 \left| \int_{-\infty}^{\infty} \psi_f^\dagger \left(\frac{e_y \Delta_y \sigma_z}{\sqrt{\Delta_y^2 + \Delta_z^2}} \right) \psi_i dx \right| \delta_{k_{y,i}, k_{y,f}}, \quad (22)$$

where $\psi_i = (\psi_{I,i}, \psi_{II,i})$, $\psi_f = (\psi_{I,f}, \psi_{II,f})$, $G_2 = G_1/4$, and the indices i and f correspond to the initial and final states, respectively. When the transition occurs between states of differing parities, the matrix element of transition, Eq. (19), becomes

$$|\langle f | \delta H | i \rangle| = G_2 \left| \int_{-\infty}^{\infty} \psi_f^\dagger \left(e_x \sigma_y + \frac{s_K e_y \Delta_z \sigma_x}{\sqrt{\Delta_y^2 + \Delta_z^2}} \right) \psi_i dx \right| \delta_{k_{y,i}, k_{y,f}}. \quad (23)$$

We will now analyze the optical selection rules in two distinct regimes. The first regime corresponds to the case where the dispersion lines are linear, here the electronlike branches have positive dispersion whereas the holelike branches have negative dispersion. The second regime corresponds to the case where there is a significant reconstruction of the eigenfunctions, i.e., a strong admixture of electronlike and holelike eigenfunctions [see Eqs. (14) and (15)].

In the linear dispersion regime, one can clearly see from Fig. 4 that the electronlike states are highly localized in the well regions, whereas the holelike states are highly localized in the barrier region. The overlap between electronlike and holelike states becomes increasingly small with increasing

Δ_y , which leads to all transitions between branches of positive and negative dispersion being heavily suppressed. Similar to nonrelativistic quantum wells, in our double-well system, within the linear regime, transitions between electronlike (holelike branches) branches are allowed for light polarized normal to the direction of the waveguide while for light polarized along the direction of the waveguide, these transitions rapidly become vanishingly small with increasing Δ_y .

For a massless Dirac system, in the energy range far away from an avoided crossing but in the region where the splitting between doublet states is maximal, transitions between the two guided modes comprising the doublet are only allowed for light linearly polarized normal to the direction of the waveguide. In stark contrast, in the vicinity of the avoided crossings, transitions strongly occur between the avoided crossing states for light linearly polarized along the direction of the waveguide. It should also be noted that transitions are also allowed between an avoided crossing level and the state belonging to an “opposite” parity branch (opposite parity in the large effective mass limit) which lies in between; in this instance, transitions are predominately polarized normally to the waveguide.

The energy-level splitting associated with quantum tunneling between wells and the avoided crossings associated with electron-hole repulsion can be utilized for THz applications. For the appropriate choice of parameters, the potential given by Eq. (10) can be used to create doublet states within the vicinity of graphene’s charge neutrality point with an energy-level splitting in the THz range. Similarly, the energy gap associated with avoided crossings can be engineered to fall within the THz regime. These avoided crossings would absorb in a narrow frequency range due to the presence of the van Hove singularity at the pseudogap edge. A detailed analysis of the optical selection rules shall be a topic of future study, and is beyond the scope of this paper. Our simple analysis serves to demonstrate the potentiality of double-well smooth electron waveguides as the basis of polarization sensitive THz detectors.

IV. CONCLUSION

We have found a class of 1D double-well potentials for which the 2D Dirac equation can be solved in terms of confluent Heun functions, and calculated the corresponding energy spectra. The energy-level splitting associated with electron tunneling between wells as well the electron-hole avoided crossing gap, can be controlled via the parameters of the electrostatic potential. Dipole optical transitions between the two states comprising a doublet, as well as transitions across the avoided crossing gap are both allowed, but follow drastically different polarization selection rules. For the doublet transitions, light is strongly absorbed for linear polarizations oriented normal to the waveguide. For the avoided crossing transitions, absorption of radiation polarized along the direction of the waveguide dominates. The presence of the van Hove singularity at the bottom of the pseudogaps opened in the spectrum leads to a narrow absorption peak, which can be tuned via the applied top-gate voltages to occur in the THz range.

ACKNOWLEDGMENTS

This work was supported by the EU H2020 RISE project TERASSE (H2020-MSCA-RISE-823878). R.R.H. acknowledges financial support from URCO (71 F U 3TAY18-3TAY19). The work of M.E.P. was supported by the Ministry of Science and Higher Education of Russian Federation, Goszadanie No. 2019-1246.

APPENDIX A: DOUBLE-WELL POTENTIALS LEADING TO THE CONFLUENT HEUN EQUATION

The solutions to many second-order differential equations, such as the Schrödinger equation and the 2D Dirac equation, can be obtained in terms of hypergeometric functions [5,54,57,123–126]. Indeed any second-order differential equation, possessing three regular singularities, can be re-expressed as Euler’s hypergeometric differential equation. Terminating the resulting hypergeometric series and/or utilizing their well-known connection formulas allows the eigenvalues of many potentials to be obtained. However, when considering the 2D Dirac equation for double-well potentials, the resulting second-order differential equation’s may contain more than three regular singularities. For example, four regular singularities means the differential equation can be re-expressed as Heun’s equation [127]. For the family of potentials which result in a differential equation having two regular singularities and one irregular singularity of rank 1, the second-order differential equation can be transformed into the confluent form of Heun’s equation. Indeed, reducing a system of coupled first-order differential equations to the confluent Heun equation has been exploited to solve various generalizations of the quantum Rabi model [110,128]. Despite the absence of a general connection formula, the confluent Heun functions can still serve as a powerful tool in studying confinement potentials and has been extensively applied in the fields of general relativity and quantum gravity [129].

Let us search for transformations which may be performed on the dependent and independent variables of Eq. (5), and the corresponding energy-independent potentials which allow Eq. (5) to be transformed into the confluent Heun equation. In some instances, the resulting confluent Heun series can be terminated [113], allowing a subset of the eigenvalues to be obtained exactly. In other instances, the entire energy spectrum can be obtained fully via the Wronskian method [39,46,112,128,130,131]. Similar approaches have been implemented in the nonrelativistic regime, indeed, for the Schrödinger equation there exist 35 choices for the coordinate transformation, each leading to 11 independent potentials which are exactly solvable in terms of the general Heun functions [126,132]. The Schrödinger equation also reduces to various forms of confluent Heun equations for potentials such as the Natanzon family [133] and several others [134].

The Bôcher symmetrical form of the Confluent Heun equation, also known as the generalized spheroidal equation, can be written using the notation from Ref. [113],

$$\frac{d}{d\xi} \left[(\xi^2 - 1) \frac{dy(\xi)}{d\xi} \right] + \left[-p^2(\xi^2 - 1) + 2p\beta\xi - \lambda - \frac{m^2 + s^2 + 2ms\xi}{\xi^2 - 1} \right] y(\xi) = 0, \quad (\text{A1})$$

where the regular singular points are located at $\xi = 1$ and $\xi = -1$. The first-order derivative can be removed by transforming the independent variable to $v(\xi) = y(\xi)\sqrt{1 - \xi^2}$; this allows Eq. (A1) to be written in normal symmetrical form:

$$-\frac{d^2 v(\xi)}{d\xi^2} + \left[p^2 + \frac{\lambda - 2p\beta\xi}{\xi^2 - 1} + \frac{m^2 + s^2 - 1 + 2ms\xi}{(\xi^2 - 1)^2} \right] v(\xi) = 0. \quad (\text{A2})$$

We shall now re-express Eq. (5) of the main text, into the same form as Eq. (A2). There are many transformations which may be performed on the dependent and independent variables of Eq. (5), which give rise to a second-order differential equation possessing no first-order derivative. Applying the transformation of the independent variable $\xi = \xi(Z)$ and $\psi_j = \exp[-\int \frac{1}{2}(\frac{d\Phi}{d\xi})d\xi]\Psi_{s_j, s_c}$ to the dependent variable yields

$$-\frac{d^2 \Psi_{s_j, s_c}}{d\xi^2} + \left[\frac{1}{4} \left(\frac{1}{\Phi} \frac{d\Phi}{d\xi} \right)^2 + \frac{1}{2} \frac{d}{d\xi} \left(\frac{1}{\Phi} \frac{d\Phi}{d\xi} \right) - s_c s_j \frac{1}{\Phi} \frac{dV}{d\xi} + \frac{(V - E)^2 - M^2}{\Phi^2} \right] \Psi_{s_j, s_c} = 0, \quad (\text{A3})$$

where $\Phi = \frac{d\xi(Z)}{dZ}$. If the potential is of the form

$$V = \frac{a_2 \xi^2 + a_1 \xi + a_0}{1 - \xi^2} \Phi_{\eta_1, \eta_2}, \quad (\text{A4})$$

then Eq. (A3) becomes exactly of the form of Eq. (A2), providing $\Phi_{\eta_1, \eta_2} = C_{\eta_1, \eta_2} (1 - \xi)^{\eta_1} (1 + \xi)^{\eta_2}$, and η_1 and η_2 can only take the values of 1 and 0, and C_{η_1, η_2} is a constant. Therefore, the wavefunctions can be expressed in terms of Heun Confluent functions. In general, the polynomial solutions of Eq. (A3) may be constructed about either of the two regular singularities located at $\xi = 1$ and $\xi = -1$, respectively. In some cases, they can be terminated for certain parameters of the potential, allowing some of the eigenvalues to be expressed explicitly. Thus, as mentioned in the Introduction, this family of potentials belongs to the class of quantum models which are quasixactly solvable [39,46,107–112]. If one of the regular singularities occurs at a finite value of x and another is at $x = \pm\infty$ (this occurs, e.g., for the Pöschl-Teller potential, see Appendix B), then the power series solution expanded about one singularity will rapidly diverge as it approaches the second singularity. In this instance, a second linearly independent solution can be constructed from a series expansion about the other singularity, allowing the full spectrum to be determined via the Wronskian method [46]. For the case where both singularities are at finite values of x , for example, for the potential described by Eq. (10) of the main text, then an iterative analytic continuation method is needed [119] to calculate the wave functions across the domain of x . A detailed review of the solutions to the confluent Heun equation can be found in Ref. [113].

As mentioned in the main text, we have restricted η_1 and η_2 to the values of zero and unity only. When $\eta_1 = \eta_2 = 1$, Eq. (A4) can be expressed as the Rosen-Morse potential, $V = b_1 \tanh^2(\tilde{x}) + b_2 \tanh(\tilde{x})$, whose eigenvalue spectrum, which is quasixact, was discussed in Ref. [46]. The

analytic bound-state energy spectra of the Rosen-Morse potential for the 2D Dirac problem has also been obtained via the Nikiforov-Uvarov method [135]. When $\eta_1 \neq \eta_2$, Eq. (A4) can be expressed as a generalized Hulthen-like potential,

$$V = \frac{c_1 \exp(-2\lambda Z) + c_2 \exp(-\lambda Z) + c_3}{1 + c_4 \exp(-\lambda Z)}, \quad (\text{A5})$$

where λ and $c_{1,2,3,4}$ are constants. When $c_1 = 0$ and $c_4 = -1$, Eq. (A5) becomes a linear combination of the Hulthen potential [136] and its logarithmic derivative. The Hulthen potential has previously been investigated for the 2D Dirac equation using an algebraic approach [137]. The case where Eq. (A5) reduces to a single exponential has also been studied in graphene waveguides [38]. It should also be noted that when $\Phi = i$, the potential given by Eq. (A4) can be reduced to the shifted 1D Coulomb potential, which has applications to charged impurities and excitons in carbon nanotubes [40].

Let us move to the case of $\eta_1 = \eta_2 = 0$, which corresponds to the potential described by Eq. (10) in the main text of the paper. In this case, it is convenient to use the nonsymmetrical canonical form of the confluent Heun equation. Expressing Ψ_{s_j, s_c} in the form of

$$\Psi_{s_j, s_c}(\xi) = (1 - \xi)^{\frac{\gamma}{2}} (1 + \xi)^{\frac{\delta}{2}} e^{-p\xi} u\left(\frac{1 - \xi}{2}\right), \quad (\text{A6})$$

and making the change of variable $\tilde{\xi} = (1 - \xi)/2$ allows Eq. (A3) to be written as

$$\frac{\partial^2 u(\tilde{\xi})}{\partial \tilde{\xi}^2} + \left(4p + \frac{\gamma}{\tilde{\xi}} + \frac{\delta}{\tilde{\xi} - 1} \right) \frac{\partial u(\tilde{\xi})}{\partial \tilde{\xi}} + \frac{4p\alpha\tilde{\xi} - \sigma}{\tilde{\xi}(\tilde{\xi} - 1)} u(\tilde{\xi}) = 0, \quad (\text{A7})$$

where

$$\gamma = m + s + 1, \quad \delta = m - s + 1,$$

$$\alpha = -\beta + m + 1, \quad \sigma = \lambda - 2p(\beta - \gamma) - m(m + 1),$$

and $u = u(p, \alpha, \gamma, \delta, \sigma; \tilde{\xi})$ are the Heun Confluent functions [113]. Currently, there are no universal expressions for arbitrary parameters connecting Heun functions about different singular points, and unlike for Gauss hypergeometric functions, there are no expressions relating the derivative of a confluent Heun function to another confluent Heun function, although particular instances have been obtained [46,138,139]. The dearth of connection formulas makes obtaining the analytic expressions for the complete eigenvalue spectrum of a wave function expressed in terms of a confluent Heun function nontrivial. However, for the potential, Eq. (10), the derivative can be expressed exactly in terms of the Heun confluent function with new parameters. Using the definition of the Heun confluent function [113], Ψ_{s_j, s_c} can be expressed in terms Ψ_{-s_j, s_c} via the relation

$$-\frac{1}{M} \left[(V - E)\Psi_{s_j, s_c} + s_j i \frac{d\Psi_{s_j, s_c}}{dx} \right] = \left(-\frac{s_a + A_0 + i s_c A_1}{2M} \right)^{-s_j s_c s_a} \Psi_{-s_j, s_c}, \quad (\text{A8})$$

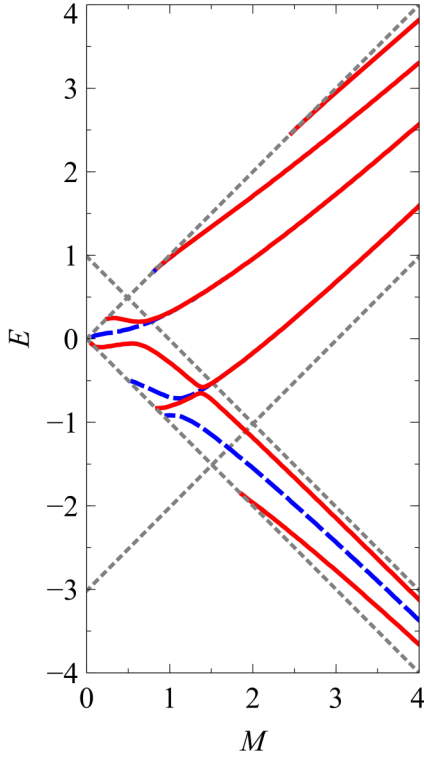


FIG. 5. The energy spectrum of bound states contained within a Rosen-Morse-double-well potential, defined by the potential parameters (a) $B_1 = 14$ and $B_2 = -1$, as a function of effective mass, M . Here, only the four lowest doublet states are displayed, while all barrier states are present within the energy range shown. The alternating red solid and blue dashed lines represent the even (odd) and odd (even) modes of ψ_I (ψ_{II}), respectively. The boundary at which the bound states merge with the continuum is denoted by the grey short dashed lines.

which allows the solution to Eq. (5) of the main text, for ψ_1 and its corresponding ψ_2 to be written as

$$\psi_1 = \sum_{s_c, c_p, s_a} C_{s_c, c_p, s_a} \left(-\frac{s_a + A_0 + i s_c A_1}{2M} \right)^{-\frac{s_c s_a}{2}} \Psi_{-1, s_c} \quad (\text{A9})$$

and

$$\psi_2 = \sum_{s_c, c_p, s_a} C_{s_c, c_p, s_a} \left(-\frac{s_a + A_0 + i s_c A_1}{2M} \right)^{\frac{s_c s_a}{2}} \Psi_{1, s_c}, \quad (\text{A10})$$

respectively, where $m = s_a A_0$, $s = i s_a (A_1 + i s_j) s_c$, and C_{s_c, c_p, s_a} are weighting coefficients. It should be noted that if m and s are exchanged, then the phase factor appearing in Eq. (A8) and Eq. (A10) must be multiplied by the factor $4^{s_c s_a}$.

APPENDIX B: EXPONENTIALLY DECAYING DOUBLE WELL

Although the double well constructed from the potential Eq. (10) is smooth and continuous across the whole of configuration space, the absolute value of the argument of the Heun function appearing in Eq. (A6) exceeds unity. Therefore, analytic continuation is needed to analyze its far-field behavior. In contrast, the corresponding Heun function for the

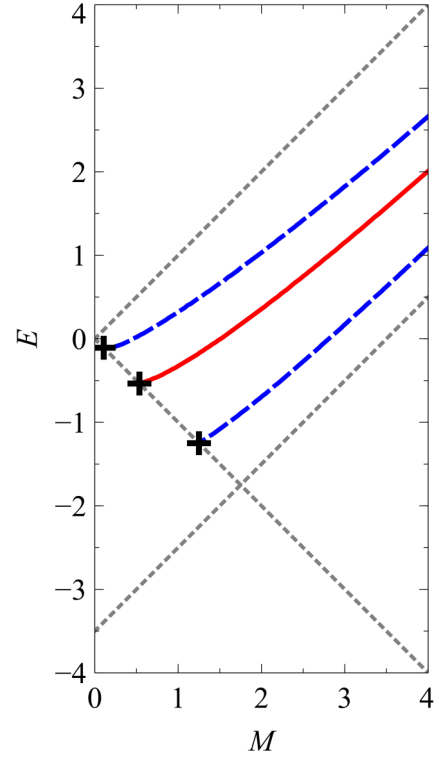


FIG. 6. The energy spectrum for the three lowest-energy guided modes contained with a Lorentzian potential of strength $A_0 = -3.5$, as a function of M . The alternating red solid and blue dashed lines represent the even (odd) and odd (even) modes of Ψ_I (Ψ_{II}), respectively. The black crosses denote the supercritical states. The boundary at which the bound states merge with the continuum is denoted by the grey short dashed lines.

Rosen-Morse potential,

$$V = -\frac{B_1}{4} [1 - \tanh^2(\tilde{x})] - \frac{B_2}{2} [1 - \tanh(\tilde{x})], \quad (\text{B1})$$

is maximally one, and therefore its far-field behavior can be determined by the expansion about the second pole [46]. Using the coordinate transformation, $\tilde{x} \rightarrow |x'| - d$, allows the Rosen-Morse potential to model a double well centered about $|x'| = 0$. Although this potential is continuous, it is not smooth. However, in the limit that $\tanh(d) \approx 1$, the discontinuity in its derivative becomes vanishingly small, making it quasismooth. This potential has the additional advantage that it can also be used to model shallow double wells. The potential parameters B_1 and B_2 appearing in Eq. (B1) are related to the parameters in Eq. (A2) via the relations

$$p = -i s_p s_c \frac{B_1}{4}, \quad \beta = -s_c s_p \left(s_j - i \frac{B_2}{2} \right),$$

$$\lambda = -\left(i s_j + \frac{B_2}{2} \right) \frac{B_2}{2} + 2 \left(E + \frac{B_2}{2} \right) \frac{B_1}{4},$$

$$s = \frac{B_2}{2m} \left(\frac{B_2}{2} + E \right),$$

$$m = \frac{s_M}{2} \{ \sqrt{M^2 - E^2} + s_m \sqrt{M^2 - (B_2 + E)^2} \},$$

where $s_M, s_m = \pm 1$ and the spinor components are given by the expressions

$$\psi_j = \sum_{s_M} \tilde{D}_{s_M} (1 - \xi)^{\frac{\gamma-1}{2}} (1 + \xi)^{\frac{\delta-1}{2}} e^{-p\xi} u\left(\frac{1 - \xi}{2}\right), \quad (\text{B2})$$

where $\xi = \tanh(\tilde{x})$. As $x \rightarrow \infty$, $\xi \rightarrow 1$, therefore s_M must be equal to 1 for the functions to decay at infinity. The bound

states are obtained via the zeros of the functions $\psi_{II}(\tilde{x}' = 0)$ and $\psi_{II}(\tilde{x}' = 0)$. In Fig. 5, we plot the energy eigenvalue spectrum for the potential, Eq. (B1), defined by the potential parameters $B_1 = 14$ and $B_2 = -1$, displaying the four lowest doublet states and complete set of barrier states within the energy range displayed.

APPENDIX C: LORENTZIAN POTENTIAL

When $p = 0$, i.e., $|E| = M$ and $A_1 = 0$, the Heun confluent function appearing in Eq. (A6) reduces to a Gauss hypergeometric function, therefore

$$u(\tilde{\xi}) = (1 - \tilde{\xi})^{-\omega} {}_2F_1\left(-s_a(s_c s_j + A_0) + \omega, \omega; \gamma, \frac{\tilde{\xi}}{\tilde{\xi} - 1}\right), \quad (\text{C1})$$

where $\omega = s_a A_0 + (1 + s_\omega \sqrt{1 + 8EA_0})/2$ and ${}_2F_1$ is the hypergeometric function. The particular case of $A_1 = 0$ corresponds to the Lorentzian potential, which notably admits exact eigenvalues for supercritical states. The emergence of a supercritical state (i.e., bound states with energy $E = -M$) is characterized by the appearance of a new node at infinity [46] as $\tilde{x}' \rightarrow \infty$, ψ_j takes the form of

$$\lim_{x \rightarrow \infty} (\psi_j) \propto R^{\frac{m+s+1}{2}} \left[\sum_{s_l} (1 - R)^{-\frac{1+\Omega_l}{2}} \frac{\Gamma(1 + s_a A_0 - s_a s_j s_c) \Gamma(\Omega_l)}{\Gamma(s_a A_0 + \frac{1+\Omega_l}{2}) \Gamma(\frac{1+\Omega_l}{2} - s_a s_c s_j)} \right], \quad (\text{C2})$$

where $\Omega_l = s_l s_\omega \sqrt{1 + 8EA_0}$, $s_l = \pm 1$ and $R = \tilde{\xi}/(\tilde{\xi} - 1)$. It can be seen from Eq. (C2) that the bound-state condition is contingent upon the value of Ω_l . For the case of $\text{Im}(\Omega_l) = 0$ and $|\Omega_l| > 1$, bound states arise when

$$E = \frac{A_0^2 + s_a(2n + 1)A_0 + n(n + 1)}{2A_0},$$

where $s_a A_0 < 0$ and $n = 0, 1, 2, \dots$ and n is restricted such that $n < |s_a A_0| - 1$. In Fig. 6, we plot the energy eigenvalue spectrum for the case of the Lorentzian potential with potential strength $A_0 = -3.5$. The exact supercritical eigenvalues are indicated by black crosses.

-
- [1] N. Rosen and P. M. Morse, On the vibrations of polyatomic molecules, *Phys. Rev.* **42**, 210 (1932).
- [2] G. J. Milburn, J. Corney, E. M. Wright, and D. F. Walls, Quantum dynamics of an atomic Bose-Einstein condensate in a double-well potential, *Phys. Rev. A* **55**, 4318 (1997).
- [3] H. J. W. Muller-Kirsten, *Introduction to Quantum Mechanics: Schrödinger Equation and Path Integral Second Edition* (World Scientific Publishing Company, Singapore, 2012).
- [4] E. Gildener and A. Patrascioiu, Pseudoparticle contributions to the energy spectrum of a one-dimensional system, *Phys. Rev. D* **16**, 423 (1977).
- [5] L. D. Landau and E. M. Lifshitz, *Quantum Mechanics: Non-relativistic Theory* (Elsevier, Oxford, 2013).
- [6] T. O. Wehling, A. M. Black-Schaffer, and A. V. Balatsky, Dirac materials, *Adv. Phys.* **63**, 1 (2014).
- [7] B. Huard, J. A. Sulpizio, N. Stander, K. Todd, B. Yang, and D. Goldhaber-Gordon, Transport Measurements Across a Tunable Potential Barrier in Graphene, *Phys. Rev. Lett.* **98**, 236803 (2007).
- [8] B. Özyilmaz, P. Jarillo-Herrero, D. Efetov, D. A. Abanin, L. S. Levitov, and P. Kim, Electronic Transport and Quantum Hall Effect in Bipolar Graphene P-N-P Junctions, *Phys. Rev. Lett.* **99**, 166804 (2007).
- [9] R. V. Gorbachev, A. S. Mayorov, A. K. Savchenko, D. W. Horsell, and F. Guinea, Conductance of p-n-p graphene structures with “air-bridge” top gates, *Nano Lett.* **8**, 1995 (2008).
- [10] G. Liu, J. Velasco, Jr., W. Bao, and C. N. Lau, Fabrication of graphene p-n-p junctions with contactless top gates, *Appl. Phys. Lett.* **92**, 203103 (2008).
- [11] J. R. Williams, T. Low, M. S. Lundstrom, and C. M. Marcus, Gate-controlled guiding of electrons in graphene, *Nat. Nanotechnol.* **6**, 222 (2011).
- [12] P. Rickhaus, M.-H. Liu, P. Makk, R. Maurand, S. Hess, S. Zihlmann, M. Weiss, K. Richter, and C. Schönenberger, Guiding of electrons in a few-mode ballistic graphene channel, *Nano Lett.* **15**, 5819 (2015).
- [13] A. Cheng, T. Taniguchi, K. Watanabe, P. Kim, and J.-D. Pillet, Guiding Dirac Fermions in Graphene with a Carbon Nanotube, *Phys. Rev. Lett.* **123**, 216804 (2019).
- [14] A. De Martino, L. Dell’Anna, and R. Egger, Magnetic Confinement of Massless Dirac Fermions in Graphene, *Phys. Rev. Lett.* **98**, 066802 (2007).
- [15] M. Ramezani Masir, A. Matulis, and F. M. Peeters, Quasi-bound states of Schrödinger and Dirac electrons in a magnetic quantum dot, *Phys. Rev. B* **79**, 155451 (2009).

- [16] P. Roy, T. K. Ghosh, and K. Bhattacharya, Localization of Dirac-like excitations in graphene in the presence of smooth inhomogeneous magnetic fields, *J. Phys. Condens. Matter* **24**, 055301 (2012).
- [17] C. A. Downing and M. E. Portnoi, Massless Dirac fermions in two dimensions: Confinement in nonuniform magnetic fields, *Phys. Rev. B* **94**, 165407 (2016).
- [18] C. A. Downing and M. E. Portnoi, Magnetic quantum dots and rings in two dimensions, *Phys. Rev. B* **94**, 045430 (2016).
- [19] N. M. R. Peres, Scattering in one-dimensional heterostructures described by the Dirac equation, *J. Phys. Condens. Matter* **21**, 095501 (2009).
- [20] A. Raoux, M. Polini, R. Asgari, A. R. Hamilton, R. Fazio, and A. H. MacDonald, Velocity-modulation control of electron-wave propagation in graphene, *Phys. Rev. B* **81**, 073407 (2010).
- [21] A. Concha and Z. Tešanović, Effect of a velocity barrier on the ballistic transport of Dirac fermions, *Phys. Rev. B* **82**, 033413 (2010).
- [22] C. A. Downing and M. E. Portnoi, Localization of massless Dirac particles via spatial modulations of the Fermi velocity, *J. Phys. Condens. Matter* **29**, 315301 (2017).
- [23] C. A. Downing and M. E. Portnoi, Trapping charge carriers in low-dimensional Dirac materials, *Int. J. Nanosci.* **18**, 1940001 (2019).
- [24] J. M. Pereira, Jr., V. Mlinar, F. M. Peeters, and P. Vasilopoulos, Confined states and direction-dependent transmission in graphene quantum wells, *Phys. Rev. B* **74**, 045424 (2006).
- [25] V. V. Cheianov, V. Fal'ko, and B. L. Altshuler, The focusing of electron flow and a Veselago lens in graphene p-n junctions, *Science* **315**, 1252 (2007).
- [26] P. G. Silvestrov and K. B. Efetov, Quantum Dots in Graphene, *Phys. Rev. Lett.* **98**, 016802 (2007).
- [27] T. Y. Tudorovskiy and A. V. Chaplik, Spatially inhomogeneous states of charge carriers in graphene, *JETP Lett.* **84**, 619 (2007).
- [28] A. V. Shytov, M. S. Rudner, and L. S. Levitov, Klein Backscattering and Fabry-Pérot Interference in Graphene Heterojunctions, *Phys. Rev. Lett.* **101**, 156804 (2008).
- [29] C. W. J. Beenakker, R. A. Sepkhanov, A. R. Akhmerov, and J. Tworzydło, Quantum Goos-Hänchen effect in graphene, *Phys. Rev. Lett.* **102**, 146804 (2009).
- [30] F.-M. Zhang, Y. He, and X. Chen, Guided modes in graphene waveguides, *Appl. Phys. Lett.* **94**, 212105 (2009).
- [31] A. Matulis and F. M. Peeters, Quasibound states of quantum dots in single and bilayer graphene, *Phys. Rev. B* **77**, 115423 (2008).
- [32] J. H. Bardarson, M. Titov, and P. W. Brouwer, Electrostatic Confinement of Electrons in an Integrable Graphene Quantum Dot, *Phys. Rev. Lett.* **102**, 226803 (2009).
- [33] L. Zhao and S. F. Yelin, Proposal for graphene-based coherent buffers and memories, *Phys. Rev. B* **81**, 115441 (2010).
- [34] Y. He, Y. Xu, Y. Yang, and W. Huang, Guided modes in asymmetric graphene waveguides, *Appl. Phys. A* **115**, 895 (2014).
- [35] P. Recher and B. Trauzettel, Quantum dots and spin qubits in graphene, *Nanotechnology* **21**, 302001 (2010).
- [36] R. R. Hartmann, N. J. Robinson, and M. E. Portnoi, Smooth electron waveguides in graphene, *Phys. Rev. B* **81**, 245431 (2010).
- [37] C. A. Downing, D. A. Stone, and M. E. Portnoi, Zero-energy states in graphene quantum dots and rings, *Phys. Rev. B* **84**, 155437 (2011).
- [38] D. A. Stone, C. A. Downing, and M. E. Portnoi, Searching for confined modes in graphene channels: The variable phase method, *Phys. Rev. B* **86**, 075464 (2012).
- [39] R. R. Hartmann and M. E. Portnoi, Quasi-exact solution to the Dirac equation for the hyperbolic-secant potential, *Phys. Rev. A* **89**, 012101 (2014).
- [40] C. A. Downing and M. E. Portnoi, One-dimensional Coulomb problem in Dirac materials, *Phys. Rev. A* **90**, 052116 (2014).
- [41] H. Hasegawa, Bound states of the one-dimensional Dirac equation for scalar and vector double square-well potentials, *Phys. E Low Dimens. Syst. Nanostruct.* **59**, 192 (2014).
- [42] Y. Xu and L. K. Ang, Guided modes in a triple-well graphene waveguide: Analogy of five-layer optical waveguide, *J. Opt.* **17**, 035005 (2015).
- [43] Y. Xu and L. K. Ang, Guided modes in a double-well asymmetric potential of a graphene waveguide, *Electronics* **5**, 87 (2016).
- [44] C. A. Downing, A. R. Pearce, R. J. Churchill, and M. E. Portnoi, Optimal traps in graphene, *Phys. Rev. B* **92**, 165401 (2015).
- [45] J. Lee, D. Wong, J. Velasco, Jr., J. F. Rodriguez-Nieva, S. Kahn, H.-Z. Tsai, T. Taniguchi, K. Watanabe, A. Zettl, F. Wang *et al.*, Imaging electrostatically confined Dirac fermions in graphene quantum dots, *Nat. Phys.* **12**, 1032 (2016).
- [46] R. R. Hartmann and M. E. Portnoi, Two-dimensional Dirac particles in a Pöschl-Teller waveguide, *Sci. Rep.* **7**, 11599 (2017).
- [47] K.-K. Bai, J.-J. Zhou, Y.-C. Wei, J.-B. Qiao, Y.-W. Liu, H.-W. Liu, H. Jiang, and L. He, Generating atomically sharp p-n junctions in graphene and testing quantum electron optics on the nanoscale, *Phys. Rev. B* **97**, 045413 (2018).
- [48] O. Klein, The reflection of electrons at a potential jump to the relative dynamics of Dirac, *Z. Phys.* **53**, 157 (1929).
- [49] M. I. Katsnelson, K. S. Novoselov, and A. K. Geim, Chiral tunneling and the Klein paradox in graphene, *Nat. Phys.* **2**, 620 (2006).
- [50] C. G. Adler, The relativistic one-dimensional square potential, *Am. J. Phys.* **39**, 305 (1971).
- [51] S.-H. Dong, X.-W. Hou, and Z.-Q. Ma, Relativistic Levinson theorem in two dimensions, *Phys. Rev. A* **58**, 2160 (1998).
- [52] N. Dombey and A. Calogeracos, Seventy years of the Klein paradox, *Phys. Rep.* **315**, 41 (1999).
- [53] N. Dombey, P. Kennedy, and A. Calogeracos, Supercriticality and Transmission Resonances in the Dirac Equation, *Phys. Rev. Lett.* **85**, 1787 (2000).
- [54] P. Kennedy, The woods-saxon potential in the Dirac equation, *J. Phys. A* **35**, 689 (2002).
- [55] V. M. Villalba and W. Greiner, Transmission resonances and supercritical states in a one-dimensional cusp potential, *Phys. Rev. A* **67**, 052707 (2003).
- [56] P. Kennedy, N. Dombey, and R. L. Hall, Phase shifts and resonances in the Dirac equation, *Int. J. Mod. Phys. A* **19**, 3557 (2004).
- [57] J. Y. Guo, Y. Yu, and S. W. Jin, Transmission resonance for a Dirac particle in a one-dimensional Hulthén potential, *Cent. Eur. J. Phys.* **7**, 168 (2009).

- [58] D. S. Miserev, Analytical study of bound states in graphene nanoribbons and carbon nanotubes: The variable phase method and the relativistic Levinson theorem, *J. Exp. Theor. Phys.* **122**, 1070 (2016).
- [59] C. L. Roy and A. Khan, Relativistic impacts on tunneling through multi-barrier systems, *J. Phys. Condens. Matter* **5**, 7701 (1993).
- [60] V. V. Cheianov and V. I. Fal'ko, Selective transmission of Dirac electrons and ballistic magnetoresistance of n-p junctions in graphene, *Phys. Rev. B* **74**, 041403(R) (2006).
- [61] Y. Jiang, S.-H. Dong, A. Antillón, and M. Lozada-Cassou, Low momentum scattering of the Dirac particle with an asymmetric cusp potential, *Eur. Phys. J. C* **45**, 525 (2006).
- [62] C. Bai and X. Zhang, Klein paradox and resonant tunneling in a graphene superlattice, *Phys. Rev. B* **76**, 075430 (2007).
- [63] M. Barbier, F. M. Peeters, P. Vasilopoulos, and J. M. Pereira Jr, Dirac and Klein-Gordon particles in one-dimensional periodic potentials, *Phys. Rev. B* **77**, 115446 (2008).
- [64] V. H. Nguyen, A. Bournel, V. L. Nguyen, and P. Dollfus, Resonant tunneling and negative transconductance in single barrier bilayer graphene structure, *Appl. Phys. Lett.* **95**, 232115 (2009).
- [65] M. Barbier, P. Vasilopoulos, and F. M. Peeters, Dirac electrons in a Kronig-Penney potential: Dispersion relation and transmission periodic in the strength of the barriers, *Phys. Rev. B* **80**, 205415 (2009).
- [66] V. M. Villalba and L. A. González-Árraga, Tunneling and transmission resonances of a Dirac particle by a double barrier, *Phys. Scr.* **81**, 025010 (2010).
- [67] J. M. Pereira Jr, F. M. Peeters, A. Chaves, and G. A. Farias, Klein tunneling in single and multiple barriers in graphene, *Semicond. Sci. Technol.* **25**, 033002 (2010).
- [68] G. J. Xu, X. G. Xu, B. H. Wu, J. C. Cao, and C. Zhang, The resonant tunneling through a graphene multiquantum well system, *J. Appl. Phys.* **107**, 123718 (2010).
- [69] M. Sharma and S. Ghosh, Electron transport and Goos-Hänchen shift in graphene with electric and magnetic barriers: Optical analogy and band structure, *J. Phys. Condens. Matter* **23**, 055501 (2011).
- [70] D. S. Miserev and M. V. Entin, Quantum mechanics of graphene with a one-dimensional potential, *J. Exp. Theor. Phys.* **115**, 694 (2012).
- [71] D. Moldovan, M. Ramezani Masir, L. Covaci, and F. M. Peeters, Resonant valley filtering of massive Dirac electrons, *Phys. Rev. B* **86**, 115431 (2012).
- [72] K. J. A. Reijnders, T. Tudorovskiy, and M. I. Katsnelson, Semiclassical theory of potential scattering for massless Dirac fermions, *Ann. Phys. (NY)* **333**, 155 (2013).
- [73] B. Fallahazad, K. Lee, S. Kang, J. Xue, S. Larentis, C. Corbet, K. Kim, H. C. P. Movva, T. Taniguchi, K. Watanabe *et al.*, Gate-tunable resonant tunneling in double bilayer graphene heterostructures, *Nano Lett.* **15**, 428 (2015).
- [74] T.-C. Hsieh, M.-Y. Chou, and Y.-S. Wu, Electrical valley filtering in transition metal dichalcogenides, *Phys. Rev. Mater.* **2**, 034003 (2018).
- [75] Y. Avishai and Y. B. Band, Klein bound states in single-layer graphene, *Phys. Rev. B* **102**, 085435 (2020).
- [76] B. Brun, N. Moreau, S. Somanchi, V.-H. Nguyen, A. Mreńca-Kolasińska, K. Watanabe, T. Taniguchi, J.-C. Charlier, C. Stampfer, and B. Hackens, Optimizing Dirac fermions quasi-confinement by potential smoothness engineering, *2D Mater.* **7**, 025037 (2020).
- [77] J. M. Pereira Jr, P. Vasilopoulos, and F. M. Peeters, Graphene-based resonant-tunneling structures, *Appl. Phys. Lett.* **90**, 132122 (2007).
- [78] J. M. Pereira Jr, P. Vasilopoulos, and F. M. Peeters, Resonant tunneling in graphene microstructures, *Microelectron. J.* **39**, 534 (2008).
- [79] D. Wei-Yin, Z. Rui, X. Yun-Chang, and D. Wen-Ji, Resonant tunneling through double-barrier structures on graphene, *Chin. Phys. B* **23**, 017202 (2013).
- [80] P. Mondal, S. Ghosh, and M. Sharma, THz photodetector using sideband-modulated transport through surface states of a 3D topological insulator, *J. Phys. Condens. Matter* **31**, 495001 (2019).
- [81] H. Bahlouli, E. B. Choubabi, A. Jellal, and M. Mekkaoui, Tunneling of graphene massive Dirac fermions through a double barrier, *J. Low Temp. Phys.* **169**, 51 (2012).
- [82] A. D. Alhaidari, H. Bahlouli, and A. Jellal, Relativistic double barrier problem with three transmission resonance regions, *Adv. Theor. Math. Phys.* **2012**, 762908 (2012).
- [83] L. Brey and H. A. Fertig, Emerging Zero Modes for Graphene in a Periodic Potential, *Phys. Rev. Lett.* **103**, 046809 (2009).
- [84] C. H. Pham and V. L. Nguyen, Tunneling through finite graphene superlattices: Resonance splitting effect, *J. Phys. Condens. Matter* **27**, 095302 (2015).
- [85] Q. Wang, R. Shen, L. Sheng, B. G. Wang, and D. Y. Xing, Transient Zitterbewegung of graphene superlattices, *Phys. Rev. A* **89**, 022121 (2014).
- [86] D. Xiao, G.-B. Liu, W. Feng, X. Xu, and W. Yao, Coupled Spin and Valley Physics in Monolayers of MoS₂ and Other Group-VI Dichalcogenides, *Phys. Rev. Lett.* **108**, 196802 (2012).
- [87] S. M. Young, S. Zaheer, J. C. Y. Teo, C. L. Kane, E. J. Mele, and A. M. Rappe, Dirac Semimetal in Three Dimensions, *Phys. Rev. Lett.* **108**, 140405 (2012).
- [88] M. Z. Hasan and C. L. Kane, Colloquium: Topological insulators, *Rev. Mod. Phys.* **82**, 3045 (2010).
- [89] X.-L. Qi and S.-C. Zhang, Topological insulators and superconductors, *Rev. Mod. Phys.* **83**, 1057 (2011).
- [90] A. Zazunov, R. Egger, and A. Levy Yeyati, Low-energy theory of transport in Majorana wire junctions, *Phys. Rev. B* **94**, 014502 (2016).
- [91] A. H. Castro Neto, F. Guinea, N. M. R. Peres, K. S. Novoselov, and A. K. Geim, The electronic properties of graphene, *Rev. Mod. Phys.* **81**, 109 (2009).
- [92] R. R. Hartmann, J. Kono, and M. E. Portnoi, Terahertz science and technology of carbon nanomaterials, *Nanotechnology* **25**, 322001 (2014).
- [93] C.-C. Liu, H. Jiang, and Y. Yao, Low-energy effective Hamiltonian involving spin-orbit coupling in silicene and two-dimensional germanium and tin, *Phys. Rev. B* **84**, 195430 (2011).
- [94] P. R. Wallace, The band theory of graphite, *Phys. Rev.* **71**, 622 (1947).
- [95] S. Dutta and S. K. Pati, Novel properties of graphene nanoribbons: A review, *J. Mater. Chem.* **20**, 8207 (2010).
- [96] H.-C. Chung, C.-P. Chang, C.-Y. Lin, and M.-F. Lin, Electronic and optical properties of graphene nanoribbons in external fields, *Phys. Chem. Chem. Phys.* **18**, 7573 (2016).

- [97] M. E. Portnoi, O. V. Kibis, and M. R. Da Costa, Terahertz applications of carbon nanotubes, *Superlattices Microstruct.* **43**, 399 (2008).
- [98] R. R. Hartmann and M. E. Portnoi, *Optoelectronic Properties of Carbon-Based Nanostructures: Steering Electrons in Graphene by Electromagnetic Fields* (LAP Lambert Academic Publishing, Saarbrücken, 2011).
- [99] R. R. Hartmann, I. A. Shelykh, and M. E. Portnoi, Excitons in narrow-gap carbon nanotubes, *Phys. Rev. B* **84**, 035437 (2011).
- [100] R. R. Hartmann and M. E. Portnoi, Terahertz transitions in quasi-metallic carbon nanotubes, *IOP Conf. Ser.: Mater. Sci. Eng.* **79**, 12014 (2015).
- [101] R. R. Hartmann, V. A. Saroka, and M. E. Portnoi, Interband transitions in narrow-gap carbon nanotubes and graphene nanoribbons, *J. Appl. Phys.* **125**, 151607 (2019).
- [102] G. Giovannetti, P. A. Khomyakov, G. Brocks, P. J. Kelly, and J. van den Brink, Substrate-induced band gap in graphene on hexagonal boron nitride: Ab initio density functional calculations, *Phys. Rev. B* **76**, 073103 (2007).
- [103] R. Dutt, A. Khare, and U. P. Sukhatme, Supersymmetry, shape invariance, and exactly solvable potentials, *Am. J. Phys.* **56**, 163 (1988).
- [104] F. Cooper, A. Khare, R. Musto, and A. Wipf, Supersymmetry and the Dirac equation, *Ann. Phys. (NY)* **187**, 1 (1988).
- [105] C.-L. Ho and P. Roy, On zero energy states in graphene, *Europhys. Lett.* **108**, 20004 (2014).
- [106] A. Schulze-Halberg and P. Roy, Bound states of the two-dimensional Dirac equation for an energy-dependent hyperbolic scarf potential, *J. Math. Phys.* **58**, 113507 (2017).
- [107] A. V. Turbiner, Quantum mechanics: Problems intermediate between exactly solvable and completely unsolvable, *Zh. Eksp. Teor. Fiz.* **94**, 33 (1988) [*Sov. Phys. JETP* **67**, 230 (1988)].
- [108] A. G. Ushveridze, *Quasi-exactly Solvable Models in Quantum Mechanics* (Institute of Physics Publishing, London, 1994).
- [109] C. M. Bender and S. Boettcher, Quasi-exactly solvable quartic potential, *J. Phys. A* **31**, L273 (1998).
- [110] R. Koç, M. Koca, and H. Tütüncüler, Quasi exact solution of the Rabi Hamiltonian, *J. Phys. A* **35**, 9425 (2002).
- [111] C. A. Downing, On a solution of the Schrödinger equation with a hyperbolic double-well potential, *J. Math. Phys.* **54**, 072101 (2013).
- [112] R. R. Hartmann, Bound states in a hyperbolic asymmetric double-well, *J. Math. Phys.* **55**, 012105 (2014).
- [113] A. Ronveaux and F. M. Arscott, *Heun's Differential Equations* (Oxford University Press, Oxford, 1995).
- [114] S.-P. You, Y. He, Y.-F. Yang, and H.-F. Zhang, Modes splitting in graphene-based double-barrier waveguides, *Chin. Phys. B* **26**, 030301 (2017).
- [115] R. R. Hartmann and M. E. Portnoi, Pair states in one-dimensional Dirac systems, *Phys. Rev. A* **95**, 062110 (2017).
- [116] A. Calogeracos and N. Dombey, Strong Levinson Theorem for the Dirac Equation, *Phys. Rev. Lett.* **93**, 180405 (2004).
- [117] Z.-Q. Ma, S.-H. Dong, and L.-Y. Wang, Levinson theorem for the Dirac equation in one dimension, *Phys. Rev. A* **74**, 012712 (2006).
- [118] Q.-g. Lin, Levinson theorem for Dirac particles in one dimension, *Eur. Phys. J. D* **7**, 515 (1999).
- [119] O. V. Motygin, On evaluation of the confluent heun functions, in *2018 Days on Diffraction (DD)*, St. Petersburg, Russia (IEEE, Piscataway, NJ, 2018), p. 223.
- [120] W. H. Press, S. A. Teukolsky, B. P. Flannery, and W. T. Vetterling, *Numerical Recipes in Fortran 77*, Fortran Numerical Recipes: The Art of Scientific Computing, Vol. 1 (Cambridge University Press, Cambridge, 1992).
- [121] J. Killingbeck, Shooting methods for the Schrodinger equation, *J. Phys. A* **20**, 1411 (1987).
- [122] V. A. Saroka, R. R. Hartmann, and M. E. Portnoi, Momentum alignment and the optical valley Hall effect in low-dimensional Dirac materials, [arXiv:1811.00987](https://arxiv.org/abs/1811.00987).
- [123] P. A. Cook, Relativistic harmonic oscillators with intrinsic spin structure, *Lett. Nuovo Cimento* (1971-1985) **1**, 419 (1971).
- [124] M. Moshinsky and A. Szczepaniak, The Dirac oscillator, *J. Phys. A* **22**, L817 (1989).
- [125] N. Candemir and O. Bayrak, Massive Dirac equation in asymmetric Hulthén potential, *J. Math. Phys.* **54**, 042104 (2013).
- [126] A. M. Ishkhanyan, Schrödinger potentials solvable in terms of the general Heun functions, *Ann. Phys. (NY)* **388**, 456 (2018).
- [127] K. Heun, Zur theorie der riemann'schen functionen zweiter ordnung mit vier verzweigungspunkten, *Math. Ann.* **33**, 161 (1888).
- [128] Q. Xie, H. Zhong, M. T. Batchelor, and C. Lee, The quantum Rabi model: Solution and dynamics, *J. Phys. A* **50**, 113001 (2017).
- [129] M. Hortaçsu, Heun functions and some of their applications in physics, *Adv. High Energy Phys.* **2018**, 8621573 (2018).
- [130] H. Zhong, Q. Xie, M. T. Batchelor, and C. Lee, Analytical eigenstates for the quantum Rabi model, *J. Phys. A* **46**, 415302 (2013).
- [131] A. J. Maciejewski, M. Przybylska, and T. Stachowiak, Full spectrum of the Rabi model, *Phys. Lett. A* **378**, 16 (2014).
- [132] A. M. Ishkhanyan, T. A. Shahverdyan, and T. A. Ishkhanyan, Thirty five classes of solutions of the quantum time-dependent two-state problem in terms of the general Heun functions, *Eur. Phys. J. D* **69**, 10 (2015).
- [133] A. M. Ishkhanyan, Schrödinger potentials solvable in terms of the confluent Heun functions, *Theor. Math. Phys.* **188**, 980 (2016).
- [134] A. M. Ishkhanyan and V. Krainov, Discretization of Natanzon potentials, *Eur. Phys. J. Plus* **131**, 342 (2016).
- [135] S. M. Ikhdair, Approximate solutions of the Dirac equation for the Rosen-Morse potential including the spin-orbit centrifugal term, *J. Math. Phys.* **51**, 023525 (2010).
- [136] L. Hulthen, *Ark. Mat. Astron. Fys.* **28A**, 5 (1942).
- [137] B. Roy and R. Roychoudhury, Dirac equation with Hulthen potential: An algebraic approach, *J. Phys. A* **23**, 5095 (1990).
- [138] P. P. Fiziev, Novel relations and new properties of confluent Heun's functions and their derivatives of arbitrary order, *J. Phys. A* **43**, 035203 (2009).
- [139] V. A. Shahnazaryan, T. A. Ishkhanyan, T. A. Shahverdyan, and A. M. Ishkhanyan, New relations for the derivative of the confluent Heun function, *Armen. J. Phys.* **5**, 146 (2012).